Supporting Information

Yuan et al. 10.1073/pnas.1413896112

SI Materials and Methods

Model to Describe the Minimum miRNA–ceRNA System. The parameters in the minimum miRNA–ceRNA model (Fig. 1*A*) are described as follows. Gene1 or gene2 transcribes into ceRNA1 or ceRNA2 at a rate of k_{R_1} or k_{R_2}, respectively. Free ceRNA1 (R_1) or ceRNA2 (R_2) degrades at a rate of g_{R_1} or g_{R_2} and translates to protein1 or protein2 at a rate k_{P_1} or k_{P_2}, respectively. Protein1 or protein2 degrades at a rate of g_{P_1} or g_{P_2}. miRNA transcribes at a rate of k_s, and the free miRNA (S) degrades at a rate of g_s. The free miRNA binds ceRNA1 or ceRNA2 at a rate of k_{1+} or k_{2+} to form a C_1 or C_2 complex, respectively. The miRNA–ceRNA1 (C_1) or miRNA–ceRNA2 (C_2) complex dissociates at a rate of k_{1-} or k_{2-} or degrades at a rate of g_1 or g_2, respectively. Along with the degradation, miRNA degrades with α_1 or α_2 possibility.

We describe the minimum miRNA–ceRNA model in Fig. 1*A*, using a set of differential equations as follows:

$$\frac{dS}{dt}=k_s-g_sS-S(k_{1+}R_1+k_{2+}R_2)+k_{1-}C_1+k_{2-}C_2 + (1-\alpha_1)g_1C_1+(1-\alpha_2)g_2C_2,$$

$$\frac{dR_1}{dt}=k_{R_1}-g_{R_1}R_1-k_{1+}SR_1+k_{1-}C_1,$$

$$\frac{dC_1}{dt}=k_{1+}SR_1-k_{1-}C_1-g_1C_1,$$

$$\frac{dR_2}{dt}=k_{R_2}-g_{R_2}R_2-k_{2+}SR_2+k_{2-}C_2,$$

$$\frac{dC_2}{dt}=k_{2+}SR_2-k_{2-}C_2-g_2C_2.$$

Solving these equations at steady state, we get

$$R_1=\frac{1}{2}\left(R_1^0-\lambda_1-\theta_1+\varphi_{21}+\sqrt{\left(\left(R_1^0-\lambda_1-\theta_1+\varphi_{21}\right)^2+4\lambda_1R_1^0\right)}\right) \quad \textbf{[S1]}$$

$$R_2=\frac{1}{2}\left(R_2^0-\lambda_2-\theta_2+\varphi_{12}+\sqrt{\left(\left(R_2^0-\lambda_2-\theta_2+\varphi_{12}\right)^2+4\lambda_2R_2^0\right)}\right), \quad \textbf{[S2]}$$

where

$$R_1^0=\frac{k_{R_1}}{g_{R_1}},$$

$$\lambda_1=\frac{g_s}{\alpha_1k_{1+}}\left(\frac{k_{1-}}{g_1}+1\right),$$

$$\theta_1=\frac{k_s}{\alpha_1g_{R_1}},$$

$$\varphi_{21}=\frac{\alpha_2g_{R_2}\left(R_2^0-R_2\right)}{\alpha_1g_{R_1}},$$

$$R_2^0=\frac{k_{R_2}}{g_{R_2}},$$

$$\lambda_2=\frac{g_s}{\alpha_2k_{2+}}\left(\frac{k_{2-}}{g_2}+1\right),$$

$$\theta_2=\frac{k_s}{\alpha_2g_{R_2}},$$

$$\varphi_{12}=\frac{\alpha_1g_{R_1}\left(R_1^0-R_1\right)}{\alpha_2g_{R_2}}.$$

Lumped parameters were introduced to simplify the presentation of Eqs. **S1** and **S2**. Each of them has specific physical meanings. Assuming that g_i, g_{R_i}, g_s, k_{i-}, and α_i ($i=1$ or 2) are fixed quantities, $1/\lambda_i$ is proportional to miRNA–target association rate k_{i+}, and θ_i is proportional to miRNA transcription rate k_s. So $1/\lambda_i$ can reflect the binding strength between miRNA and ceRNA, and θ_i can reflect miRNA expression level. R_i^0 is the basal mRNA expression level when there is no miRNA regulation, and φ_{ji} represents the strength of cross-regulation on ceRNA i by ceRNA j.

The parameter α ($0\le\alpha\le1$) represents the probability that a miRNA is consumed after degrading its target. The expected number of target RNA molecules that one miRNA molecule can degrade is $\lim_{K\to\infty}\sum_{k=1}^{K}k\alpha(1-\alpha)^{k-1}=1/\alpha$. It is easier to estimate the circulation capacity of miRNAs by using their loss rates, rather than by using their recycling rates ($1-\alpha$). Therefore, we used the miRNA loss rate instead of the recycling rate, to represent miRNA circulation capacity.

Effect of Endogenous Targets. To gain insight about the effect of the endogenous miR-21 targets on the synthetic minimum ceRNA system, we treated all of the endogenous miR-21 targets as a pool and modeled them as a third ceRNA species in the model. Thus, we expanded the equations as follows:

$$\frac{dS}{dt}=k_s-g_sS-S(k_{1+}R_1+k_{2+}R_2+k_{3+}R_3) + k_{1-}C_1+k_{2-}C_2+k_{3-}C_3+(1-\alpha_1)g_1C_1 + (1-\alpha_2)g_2C_2+(1-\alpha_3)g_3C_3,$$

$$\frac{dR_1}{dt}=k_{R_1}-g_{R_1}R_1-k_{1+}SR_1+k_{1-}C_1,$$

$$\frac{dC_1}{dt}=k_{1+}SR_1-k_{1-}C_1-g_1C_1,$$

$$\frac{dR_2}{dt}=k_{R_2}-g_{R_2}R_2-k_{2+}SR_2+k_{2-}C_2,$$

$$\frac{dC_2}{dt}=k_{2+}SR_2-k_{2-}C_2-g_2C_2,$$

$$\frac{dR_3}{dt}=k_{R_3}-g_{R_3}R_3-k_{3+}SR_3+k_{3-}C_3,$$

$$\frac{dC_3}{dt} = k_{3+}SR_3 - k_{3-}C_3 - g_3C_3.$$

Solving these equations at steady state, we get

$$R_1 = \frac{1}{2}\left(R_1^0 - \lambda_1 - \theta_1' + \varphi_{21} + \sqrt{\left(\left(R_1^0 - \lambda_1 - \theta_1' + \varphi_{21}\right)^2 + 4\lambda_1 R_1^0\right)}\right)$$

$$R_2 = \frac{1}{2}\left(R_2^0 - \lambda_2 - \theta_2' + \varphi_{12} + \sqrt{\left(\left(R_2^0 - \lambda_2 - \theta_2' + \varphi_{12}\right)^2 + 4\lambda_2 R_2^0\right)}\right), \quad \textbf{[S3]}$$

where

$$R_1^0 = \frac{k_{R_1}}{g_{R_1}}, \quad R_2^0 = \frac{k_{R_2}}{g_{R_2}},$$

$$\lambda_1 = \frac{g_s}{\alpha_1 k_{1+}}\left(\frac{k_{1-}}{g_1} + 1\right), \quad \lambda_2 = \frac{g_s}{\alpha_2 k_{2+}}\left(\frac{k_{2-}}{g_2} + 1\right),$$

$$\theta_1 = \frac{k_s}{\alpha_1 g_{R_1}}, \quad \theta_2 = \frac{k_s}{\alpha_2 g_{R_2}},$$

$$\varphi_{21} = \frac{\alpha_2 g_{R_2}\left(R_2^0 - R_2\right)}{\alpha_1 g_{R_1}}, \quad \varphi_{12} = \frac{\alpha_1 g_{R_1}\left(R_1^0 - R_1\right)}{\alpha_2 g_{R_2}},$$

$$\varphi_{31} = \frac{\alpha_3 g_{R_3}\left(R_3^0 - R_3\right)}{\alpha_1 g_{R_1}}, \quad \varphi_{32} = \frac{\alpha_3 g_{R_3}\left(R_3^0 - R_3\right)}{\alpha_2 g_{R_2}},$$

$$\theta_1' = \theta_1 - \varphi_{31} = \frac{k_s - \alpha_3 g_{R_3}\left(R_3^0 - R_3\right)}{\alpha_1 g_{R_1}} = \frac{k_s'}{\alpha_1 g_{R_1}},$$

$$\theta_2' = \theta_2 - \varphi_{32} = \frac{k_s - \alpha_3 g_{R_3}\left(R_3^0 - R_3\right)}{\alpha_2 g_{R_2}} = \frac{k_s'}{\alpha_2 g_{R_2}}.$$

The form of Eq. **S3** is almost identical to that of Eqs. **S1** and **S2**. The existence of endogenous targets simply rescaled the parameter θ, which represented the effective miRNA level.

Model-Fitting Strategy. For the ease of description, we used subscript m to represent mKate, subscript t to represent TagBFP, and subscript e to represent EYFP. M represents the free mRNA level.

As shown in Fig S1*B*, the TagBFP fluorescent mean values were linearly correlated with the EYFP and mKate mean values by using binning analysis, respectively. In addition, the fluorescence values were linearly correlated with the mRNA expression levels, respectively (Fig. S1 *C*–*E*). Thus, we reasoned that the TagBFP fluorescent value could be used to estimate the transcriptional levels of ceRNA1 and ceRNA2 in our experiments. As the florescent value measured by the flow cytometer was in an arbitrary unit, the absolute protein value between different channels was not directly comparable. The slope of the linear correlation between these protein values could be different. We took this property into account in our model as described below.

Estimate mRNA level by fluorescent value. Based on results shown in Fig. S1*C*, we modeled the relationship between the TagBFP fluorescent value and the mRNA concentration, using the formula

$$\log_{10}\left(\frac{F_t}{F_t^0}\right) = K_t \log_{10}\left(\frac{M_t}{M_t^0}\right) + b_t, \quad \textbf{[S4]}$$

where M_t is the concentration of TagBFP mRNA molecules, M_t^0 is a benchmark concentration of TagBFP mRNA molecules, F_t is the TagBFP fluorescent value, F_t^0 is the benchmark fluorescent value, K_t is the slope, and b_t is the intercept. Based on Eq. **S4**, we get

$$\log_{10}(F_t) = K_t \log_{10}(M_t) + B_t, \quad \text{where } B_t = b_t + \log_{10}\left(F_1^0\right) - K_t \log_{10}\left(M_t^0\right). \quad \textbf{[S5]}$$

Based on Eq. **S5**, we estimated the TagBFP mRNA level as a function of its fluorescent value as follows:

$$M_t = 10^{\left(\left(\log_{10}(F_t) - B_t\right)/K_t\right)}. \quad \textbf{[S6]}$$

We estimated the range of K_t based on the slope shown in Fig S1*F* and estimated that of B_t as the fluorescent value that separates the background and foreground cell populations. We estimated the parameters for iRFP, mKate, and EYFP, using the same methods as described above.

Use of TagBFP fluorescent level to represent ceRNA transcriptional level. We used a simple kinetic model to describe the mRNA level driven by a constitutive promoter,

$$\frac{dM}{dt} = k - gM,$$

where k is transcriptional rate, g is the degradation rate, and M is the mRNA level. At steady state, $M = k/g$.

As mKate (ceRNA1), EYFP (ceRNA2), and TagBFP were all driven by constitutive promoters, the transcription levels of mKate and EYFP were linearly correlated to the mRNA level of TagBFP at steady state,

$$k_m = K_1 g_m M_t, \quad k_e = K_2 g_e M_t, \quad \textbf{[S7]}$$

where, K_1 and K_2 are constants that reflect relative transcription rate.

From Eqs. **S5** and **S7**, we get

$$\log_{10}(F_m) = \frac{K_m}{K_t}\log_{10}(\mathrm{F}_t) + \log_{10}(K_1) - \frac{B_t}{K_t} + \frac{B_m}{K_m},$$

$$\log_{10}(F_e) = \frac{K_e}{K_t}\log_{10}(\mathrm{F}_t) + \log_{10}(K_2) - \frac{B_t}{K_t} + \frac{B_e}{K_e}.$$

These two equations suggest that the EYFP and mKate fluorescent values are positively and linearly correlated with TagBFP values, and the slopes are determined by the scales of arbitrary units of these fluorescent values.

The transcriptional levels of mKate and EYFP could be represented by TagBFP fluorescent level as follows:

$$k_m = K_1 g_m 10^{\left(\left(\log_{10}(F_t) - B_t\right)/K_t\right)}, \quad k_e = K_2 g_e 10^{\left(\left(\log_{10}(F_t) - B_t\right)/K_t\right)}. \quad \textbf{[S8]}$$

From Eqs. **S8** we can get

$$\log_{10}(k_m) = \frac{1}{K_t}\log_{10}(F_t) + T_1$$

$$\log_{10}(k_e) = \frac{1}{K_t}\log_{10}(F_t) + T_2,$$

where T_1 and T_2 are constants. We can see that logarithmic-transformed TagBFP fluorescent level are linearly corrected to the log-transformed transcriptional rate of mKate and EYFP.

Thus, we reasoned that TagBFP fluorescent level could be used to indicate the transcriptional level of ceRNAs.

Parameter fitting. Based on Eqs. **S1**, **S2**, **S6**, and **S8**, we could formulate the fitting problem as

$$\log_{10}(F_m) = K_m \log_{10}\left(K_1 10^{((\log_{10}(F_t)-B_t)/K_t)} - \lambda_1 - \theta_1 + \sigma\left(K_2 10^{((\log_{10}(F_t)-B_t)/K_t)} - 10^{((\log_{10}(F_e)-B_e)/K_e)}\right) + \sqrt{\left(K_1 10^{((\log_{10}(F_t)-B_t)/K_t)} - \lambda_1 - \theta_1 + \sigma\left(K_2 10^{((\log_{10}(F_t)-B_t)/K_t)} - 10^{((\log_{10}(F_e)-B_e)/K_e)}\right)\right)^2 + 4\lambda_1 K_1 10^{((\log_{10}(F_t)-B_t)/K_t)}}\right) + B_m \quad \textbf{[S9]}$$

$$\log_{10}(F_e) = K_e \log_{10}\left(K_2 10^{((\log_{10}(F_t)-B_t)/K_t)} - \lambda_2 - \frac{\theta_1}{\sigma} + \frac{\left(K_1 10^{((\log_{10}(F_t)-B_t)/K_t)} - 10^{((\log_{10}(F_m)-B_m)/K_m)}\right)}{\sigma} + \sqrt{\left(K_2 10^{((\log_{10}(F_t)-B_t)/K_t)} - \lambda_2 - \frac{\theta_1}{\sigma} + \frac{\left(K_1 10^{((\log_{10}(F_t)-B_t)/K_t)} - 10^{((\log_{10}(F_m)-B_m)/K_m)}\right)}{\sigma}\right)^2 + 4\lambda_2 K_2 10^{((\log_{10}(F_t)-B_t)/K_t)}}\right) + B_e, \quad \textbf{[S10]}$$

where $\sigma = \alpha_2 g_{R_2}/\alpha_1 g_{R_1}$.

The parameters we need to fit are $K_t, B_t, K_e, B_e, K_m, B_m, K_1, K_2, \lambda_1, \theta_1$, and σ. We used stepwise least-squares regression to fit this model. First, we fitted the data obtained in the absence of Dox, which contain only mKate and TagBFP fluorescence data. In this case, we did not have to consider Eq. **S10**, so Eq. **S9** was simplified to the following form:

$$\log_{10}(F_m) = K_m \log_{10}\left(K_1 10^{((\log_{10}(F_t)-B_t)/K_t)} - \lambda_1 - \theta_1 + \sqrt{\left(K_1 10^{((\log_{10}(F_t)-B_t)/K_t)} - \lambda_1 - \theta_1\right)^2 + 4\lambda_1 K_1 10^{((\log_{10}(F_t)-B_t)/K_t)}}\right) + B_m. \quad \textbf{[S11]}$$

The parameters that we need to fit are $K_t, B_t, K_m, B_m, K_1, \lambda_1$, and θ_1.

Next, the mKate, TagBFP, and EYFP data from Dox+ samples were used for data fitting. The parameters that we need to fit are K_t, B_t, K_e, B_e, K_m, B_m, K_1, K_2, λ_1, θ_1, and σ, among which $K_t, B_t, K_m, B_m, K_1, \lambda_1$, and θ_1 were adopted from the first step. We used the *lsqcurvefit* function in MATLAB to fit the data. Because the fitting is in a multiple-parameter space, the results given by gradient descent algorithms might be trapped into local solutions. To overcome this problem, we started the fitting in random initial values and made the decision according to the parameter histogram.

Loss rate ratio estimation. To estimate the loss rate ratio α_2/α_1, we did the model fitting for the (partially paired EYFP)–(partially paired mKate) target pair and for the (perfectly paired EYFP)–(partially paired mKate) target pair in Fig. 5*B*. Assuming free mRNA degradation rates g_{R_1}, g_{R_2} are constant in both experiments, σ indicates the miRNA loss rate ratio α_2/α_1 of the ceRNA2–miRNA complex to the ceRNA1–miRNA complex. We assumed that all parameters in Eqs. **S9** and **S10** of the two datasets are identical, except for K_1, K_2, λ_2, and σ. Because the gradient descent algorithm used to fit parameters could be trapped into local optimal solutions, parameter fitting was conducted 1,000 times by using random initial parameter values for each case, and the most frequent value was used as the final parameter estimation.

Reagents and Enzymes. Restriction endonuclease, polynucleotide kinase (PNK), T4 DNA ligase, Quick DNA ligase, Taq DNA Polymerases, and Phusion High-Fidelity DNA polymerase were purchased from New England Biolabs. Oligonucleotides were synthesized by Sangon Biotech and Genewiz. Oligonucleotide sequences are listed in Table S1. Dox was purchased from Clontech. Gateway BP and LR reactions (Life Technologies) were performed, following the manufacturer's protocol.

Cell Transfection and Fluorescence-Activated Cell Sorting Measurement. The HEK293 cell line (Life Technologies) was grown in Dulbecco's modified Eagle's medium (DMEM) complete media [DMEM supplemented with 4.5 g/L glucose, 0.045 g/mL of penicillin, 0.045 g/mL streptomycin, and 10% (vol/vol) FBS (Life Technologies)] at 37 °C, 100% humidity and 5% CO_2. Transfection experiments were performed in 24-well plates, using Lipofectamine LTX (Life Technologies), following the manufacturer's protocol. The plasmid pDT7004 (pUBI-linker-NOS) that contains a maize ubiquitin promoter (UBI) followed by a NOS terminator (transcription terminator derived from the nopaline synthase gene from *Agrobacterium tumefaciens*) with no protein-coding sequences between UBI and NOS was used to ensure an equal amount of plasmid DNA in each experiment. The amount of plasmid DNA and the final concentration of Dox added to each well are listed in Table S2.

Cells were harvested 48 h posttransfection for flow cytometry analysis as described previously (1, 2). A Fortessa flow analyzer (BD Bioscience) was used for FACS analysis with the following settings: TagBFP was measured using a 405-nm laser and a 450/50 filter with a photomultiplier tube (PMT) at 245 V, mKate was measured with a 561-nm laser and a 670/30 filter using a PMT at 300 V, EYFP was measured with a 488-nm laser and a 530/30 filter using a PMT at 176 V, and iRFP was measured using a 640-nm laser and a 780/60 filter with a PMT at 445 V. For each sample, $\sim 5 \times 10^4$ to $\sim 1 \times 10^5$ cell events were collected.

To test whether the fluorescent value linearly correlates to the corresponding mRNA level, we cotransfected plasmids encoding TagBFP, EYFP, and mKate into HEK293 cells (Table S2 and Fig. S1). To test whether the iRFP fluorescent intensity linearly correlates to miRNA transcription level, the plasmid encoding iRFP and miR-21 was transfected into HEK293 cells (Table S2 and Fig. S1). TagBFP-positive or iRFP-positive cells were divided into seven or eight bins at equal logarithmic scales, respectively, ranging from the lowest to the highest TagBFP or iRFP values. For each bin, $\sim 1 \times 10^4$ cells were collected in DMEM complete media by using a BD

FACS Aria III cell sorter with the following configurations: TagBFP was measured using a 405-nm laser and a 450/50 filter with a PMT at 280 V, mKate was measured with a 561-nm laser and a 610/20 filter using a PMT at 330 V, EYFP was measured with a 488-nm laser and a 530/30 filter using a PMT at 250 V, and iRFP was measured using a 633-nm laser and a 780/60 filter with a PMT at 484 V.

FACS Data Processing and Model Fitting. Fluorescence compensations were subtracted from the raw FACS data (Fig. S6). TagBFP-positive cell events were gated according to the iRFP channel to make sure that the miR-21 level is roughly a constant in each TagBFP bin (Fig. S2). Then cells were sorted by TagBFP values, and every 150 cell events were grouped into each nonoverlapped bin (Fig. S1*A*). The median values of indicated fluorescent intensities in each bin were used for modeling and in scatter plots that were drawn in Matlab (MathWorks) or the R "Bioconductor" package (3).

To create a miR-21 gradient, we transfected HEK293 cells with increasing amounts of the plasmid that encodes iRFP and miR-21. Cell events whose iRFP values ranked from 45% to 70% of all TagBFP-positive events were gated for analysis. These gated cells have an approximately equal mean value of TagBFP normal distribution, but display a gradually increased mean value of iRFP normal distribution with increasing amount of the iRFP plasmid in the transfection experiment (Fig. S2). The *lsqcurvefit* function in MATLAB was used to fit model parameters.

RNA Extraction and qRT-PCR. RNA was extracted from sorted cells, using the miRNeasy Mini Kit (Qiagen). The miScript II RT Kit (Qiagen) was used for miRNA expression analysis. The real-time PCR reactions were performed in triplicate, using SYBR Select Master Mix (Life Technologies). Relative changes in gene expression were calculated using the $2^{-\Delta\Delta CT}$ method and normalized for miRNA and mRNA expression levels by using U6 and β-actin levels respectively. The primers used in qRT-PCR are listed in Table S1.

RNA Library Preparation and Sequencing. The plasmids used in Fig. S5 are listed in Table S2. TagBFP-positive cells were sorted into three bins at equal logarithmic scale 48 h posttransfection. RNA was extracted using TRIzol (Life Technologies) and mRNA isolation was performed using the NEBNext Poly(A) mRNA Magnetic Isolation kit (New England Biolabs). Reverse transcription was performed using the ProtoScript II First-Strand cDNA Synthesis Kit, and the second-strand cDNA was synthesized using the NEBNext mRNA Second-Strand Synthesis Module (New England Biolabs). The cDNA was fragmented using Covaris S220 and purified using AMPure XP Beads (Beckman Coulter). The adapter was ligated using T4 DNA ligase (Enzymatics). PCR was performed using an End Repair/dA-tail ligated DNA template to include unique barcodes for sample identification (Enzymatics). All PCR products were pooled in an equimolar ratio and sequenced on the rapid mode by using Hiseq2500 (Illumina).

RNA Sequencing Analysis. TagBFP-positive cells were sorted into three bins at equal logarithmic scale 48 h posttransfection for Dox+ and Dox− samples, respectively. Poly(A)$^+$ transcripts were isolated for HiSeq2500 (Illumina) sequencing. The Bowtie2 index was created based on the human UCSC genome and known Gene transcriptome19, and paired-end reads were aligned directly to this index using Tophat with command line options –r 500 –p 8. Next, cufflinks-2.2.1 was run with default parameters on the alignments (accepted_hits.bam) created by Tophat to estimate expression levels for each transcript [fragments per kilobase of transcript per million mapped reads (FPKM)].

Plasmid DNA Constructs.

Entry vectors.

pZ246 (pEntr_L4_MCS_R1) was made by inserting annealed oligos p1 and p2 into pENTR_L4-CMV-R1 (4).

pZ250 (pEntr_L4_CAG_R1) was made by subcloning the CAG promoter from pCAG-DsRed-FF (1) into pZ246, using PacI and EcoRI.

pZ251 (pEntr_L4_TRE_R1) was made by subcloning the TRE promoter from pTRE-LacI-FF5 (1) into pZ246 using SpeI and XhoI.

pZ451 (pEntr_L1_mKate-MCS_L2) was made by inserting a fragment containing multiple cloning sites through annealed oligos p3 and p4 into pZ258, using NotI and HindIII. pZ258 (pEntr_L1_mKate-FF5-FF4_L2) was made by inserting an FF5×4-FF4×3 fragment from pCAGop-DsRed-FF5-FF4 (1) into pZ245, using NotI and XmaI. pZ245 (pEntr-L1_mKate_NotIXmaI_L2) was made by a BP reaction with pDNOR211P1P2 (Life Technologies) and B1_mKate_NotIXmaI_B2, following the manufacturer's protocol. B1_mKate_NotIXmaI_B2 was PCR amplified from pENTR_L1_mKate_L2 (4) by using primers p5 and p6.

pZ452 (pENTR_L1_EYFP-MCS_L2) was made by inserting a fragment containing multiple cloning sites through annealed oligos p3 and p4 into pENTR_L1_EYFP-FF5_L2, using NotI and HindII. pENTR_L1_EYFP-FF5_L2 was made by inserting an EYFP fragment from pCAG-EYFP (1) into pZ263, using AgeI and NotI. pZ263 (pENTR_L1_EYFP-2A-rtTA-FF5_L2) was made by a BP reaction with pDNOR211P1P2 (Life Technologies) and B1_EYFP-2A-rtTA-FF5_B2, following the manufacturer's protocol. B1_EYFP-2A-rtTA-FF5_B2 was PCR amplified from pZ248 by using primers p7 and p8. pZ248 (pCMV-EYFP-2A-rtTA-FF5 × 4) was made by inserting a PCR fragment EYFP-2A into pCMV-rtTA-FF5×4 (1), using NheI, and the fragment was amplified from pCAG-EYFP using primers p9 and p10.

pZ443 (pENTR_L1_rtTA-2A-Puro-FF5_L2) was made by inserting a puromycin fragment into pZ305 by using SpeI and NotI. The puromycin fragment was PCR amplified from pENTR_L1_Puro_L2 (4), using primers p11 and p12. pZ305 (pENTR_L1_rtTA-2A-Hyg-FF5_L2) was made by inserting rtTA-2A into pZ294 by using AgeI and XbaI. The fragment was PCR amplified from pZ091 (pCMV-rtTA-FF5) (1), using primers p13 and p14. pZ294 (pENTR_L1_EYFP-2A-Hyg-FF5_L2) was made by inserting Hygromycin from pCMV-IRES2-Hygro into pZ263 (1) by XbaI and NotI.

pZ393 (pENTR_L1_TagBFP-FF5_L2) was made by inserting a TagBFP fragment into pZ263 by using AgeI and NotI. The TagBFP fragment was PCR amplified from pTagBFP-N purchased from Evrogen by using primers p15 and p16.

pZ323 (pENTR_L1_Cerulean-miR-21_L2) was made by inserting miR-21 into pZ310 (1) by using NotI and HindIII. The miR-21 fragment was PCR amplified from the purified human genome by using primers p17 and p18 containing an intron splice donor site in the 5′ primer and an intron splice acceptor site and a pyrimidine-rich region in the 3′ primer.

pZ508 (pCMV-iRFP) was purchased from Addgene.

pZ304 (pENTR_L1_RheoAct-2A-Rec-FF3_L2) was made by inserting the FF3×4 target site through annealed oligos p19 and p20 into pZ297 by using NotI and HindIII. pZ297 (pENTR_L1_RheoAct-2A-Rec-T294_L2) was made by subcloning RheoAct-2A-Rec from pZ208 (pCAGop-RheoAct-2A-RheoRec-FF5×4) (5) into pZ268 (1) by NcoI and NotI.

pZ296 (pEntr-L4_5xUAS_R1) was made by subcloning 5×Gal4 from pZ229 (5×Gal4-CMVmini-dsRed-FF5×4) (1) into pZ246, using PacI and EcoRI.

pB035 (pEntr_L1_EYFP-1×PDCD4_L2) was made by subcloning the 1×PDCD4 miR-21 target site from pcDNA3.1-Luc (6) into pZ452 by NotI and SalI.

pB100 (pEntr_L1_EYFP-4×PDCD4_L2) was made by inserting the 4×PDCD4 miR-21 target site through annealed oligos b13009, b13010, b13011, and b13012 into pZ452 by NotI and SalI.

pB178 (pEntr_L1_EYFP-8×PDCD4_L2) was made by inserting the 4×PDCD4 miR-21 target site through annealed oligos b13021, b13022, b13023, b13024, b13025, and b13026 into pB100 by KpnI and XmaI.

pB182 (pEntr_L1_EYFP-12×PDCD4_L2) was made by inserting the 4×PDCD4 miR-21 target site through annealed oligos b13009, b13010, b13011, and b13012 into pB178 by NotI and SalI.

pB252 (pEntr_L1_EYFP-4×BMPR2III_L2) was made by inserting the 4×BMPR2IIImiR-21 target site through annealed oligos b13070, b13071, b13072, and b13073 into pZ452 by NotI and XmaI.

pB254 (pEntr_L1_EYFP-4×MTAP_L2) was made by inserting the 4×MTAP miR-21 target site through annealed oligos b13078, b13079, b13080, and b13081 into pZ452 by NotI and XmaI.

pB256 (pEntr_L1_EYFP-4×PDCD4II_L2) was made by inserting the 4×PDCD4II miR-21 target site through annealed oligos b13086, b13087, b13088, and b13089 into pZ452 by NotI and XmaI.

pB258 (pEntr_L1_EYFP-4×PPARA_L2) was made by inserting the 4×PPARA miR-21 target site through annealed oligos b13094, b13095, b13096, and b13097 into pZ452 by NotI and XmaI.

pB260 (pEntr_L1_EYFP-4×RECKII_L2) was made by inserting the 4×RECKII miR-21 target site through annealed oligos b13102, b13103, b13104, and b13105 into pZ452 by NotI and XmaI.

pB037 (pEntr_L1_mKate-1×PDCD4_L2) was made by subcloning the 1×PDCD4 miR-21 target site from pcDNA3.1-Luc (6) into pZ451 by NotI and SalI.

pB102 (pEntr_L1_mKate-4×PDCD4_L2) was made by inserting annealed oligos b13009, b13010, b13011, and b13012 into pZ451 by NotI and SalI.

pB194 (pEntr_L1_mKate-4×PDCD4-MCS_L2) was made by inserting annealed oligos b13035 and b13036 into pB102 by KpnI.

pB179 (pEntr_L1_mKate-8×PDCD4_L2) was made by inserting the 4×PDCD4 miR-21 target site through annealed oligos b13021, b13022, b13023, b13024, b13025, and b13026 into pB194 by KpnI and XmaI.

pB183 (pEntr_L1_mKate-12×PDCD4_L2) was made by inserting annealed oligos b13009, b13010, b13011, and b13012 into pB179 by NotI and SalI.

pB261 (pEntr_L1_mKate-4×BMPR2III_L2) was made by inserting annealed oligos b13070, b13071, b13072, and b13073 into pZ451 by NotI and XmaI.

pB269 (pEntr_L1_mKate-4×RECKII_L2) was made by inserting annealed oligos b13070, b13071, b13072, and b13073 into pZ451 by NotI and XmaI.

pB045 (pEntr_L1_iRFP-miR-21_L2) was made by PCR-amplified iRFP from pZ508, using primer ch-5 and b12009 inserted into pZ323 by AgeI and NotI.

pB399 (pEntr_L1_EYFP-4×T21_L2) was made by inserting the 4×T21 miR-21 target site from pZ509 into pZ452 by NotI and HindIII. pZ509 (pEntr_L1_mKate-T21-FF4_L2) was made by inserting the 4×T21 miR-21 target site from pZ252 into pZ258 by NotI and HindIII. pZ252 (pEntr_L1_rtTA-4×T21_L2) was made by a BP reaction with pDNOR211P1P2 (Life Technologies) and B1_rtTA-4×T21_B2, following the manufacturer's protocol. B1_rtTA-4×T21_B2 was PCR amplified from pZ090 (pCMV-rtTA-T21×4) (1), using primers p21 and p22.

Expression vectors.

pB003 (pZD_Seq1-CAG-rtTA-2A-Puro-FF5-Seq2) was prepared by combining pZ250 (pENTR_L4-CAG_L1) and pZ443 (pENTR_L1-rtTA-2A-Puro-FF5_L2) with pZDonor_1-GTW-2 in a Gateway LR reaction.

pB018 (pZD_Seq5-CAG-TagBFP-FF5-Seq6) was prepared by combining pZ250 (pENTR_L4-CAG_L1) and pZ393 (pENTR_L1-TagBFP-FF5_L2) with pZDonor_5-GTW-6 in a Gateway LR reaction.

pB040 (pZD_Seq3-TRE-EYFP-1×PDCD4-Seq4) was prepared by combining pZ251 (pENTR_L4-TRE_L1) and pB035 (pENTR_L1-EYFP-1×PDCD4_L2) with pZDonor_3-GTW-4 in a Gateway LR reaction.

pB044 (pZD_Seq3-TRE-EYFP-MCS-Seq4) was prepared by combining pZ251 (pENTR_L4-TRE_L1) and pZ452 (pENTR_L1-EYFP-MCS_L2) with pZDonor_3-GTW-4 in a Gateway LR reaction.

pB104 (pZD_Seq3-TRE-EYFP-4×PDCD4-Seq4) was prepared by combining pZ251 (pENTR_L4-TRE_L1) and pB100 (pENTR_L1-EYFP-4×PDCD4_L2) with pZDonor_3-GTW-4 in a Gateway LR reaction.

pB180 (pZD_Seq3-TRE-EYFP-8×PDCD4-Seq4) was prepared by combining pZ251 (pENTR_L4-TRE_L1) and pB178 (pENTR_L1-EYFP-8×PDCD4_L2) with pZDonor_3-GTW-4 in a Gateway LR reaction.

pB184 (pZD_Seq3-TRE-EYFP-12×PDCD4-Seq4) was prepared by combining pZ251 (pENTR_L4-TRE_L1) and pB182 (pENTR_L1-EYFP-12×PDCD4_L2) with pZDonor_3-GTW-4 in a Gateway LR reaction.

pB400 (pZD_Seq3-TRE-EYFP-4×T21-Seq4) was prepared by combining pZ251 (pENTR_L4-TRE_L1) and pB399 (pENTR_L1-EYFP-4×T21_L2) with pZDonor_3-GTW-4 in a Gateway LR reaction.

pB106 (pZD_Seq2-hEF1α-mKate-4×PDCD4-Seq3) was prepared by combining pZ529 (pENTR_L4-hEF1α_L1) (4) and pB102 (pENTR_L1-mKate-4×PDCD4_L2) with pZDonor_2-GTW-3 in a Gateway LR reaction.

pB251 (pZD_Seq2-hEF1α-mKate-Seq3) was prepared by combining pZ529 (pENTR_L4-hEF1α_L1) (4) and pZ245 (pENTR_L1-mKate_L2) with pZDonor_2-GTW-3 in a Gateway LR reaction.

pB279 (pZD_Seq2-hEF1α-mKate-4×BMPR2III-Seq3) was prepared by combining pZ529 (pENTR_L4-hEF1α_L1) (4) and pB261 (pENTR_L1-mKate-4×BMPR2III_L2) with pZDonor_2-GTW-3 in a Gateway LR reaction.

pB287 (pZD_Seq2-hEF1α-mKate-4×RECKII-Seq3) was prepared by combining pZ529 (pENTR_L4-hEF1α_L1) (4) and pB269 (pENTR_L1-mKate-4×RECKII_L2) with pZDonor_2-GTW-3 in a Gateway LR reaction.

pB328 (pZD_Seq3-hEF1α-iRFP-miR-21-Seq4) was prepared by combining pZ529 (pENTR_L4-hEF1α_L1) (4) and pB045 (pENTR_L1-iRFP_L2) with pZDonor_3-GTW-4 in a Gateway LR reaction.

pB270 (pZD_Seq3-TRE-EYFP-4×BMPR2III-Seq4) was prepared by combining pZ251 (pENTR_L4-TRE_L1) and pB252 (pENTR_L1-EYFP-4×BMPR2III_L2) with pZDonor_3-GTW-4 in a Gateway LR reaction.

pB272 (pZD_Seq3-TRE-EYFP-4×MATP-Seq4) was prepared by combining pZ251 (pENTR_L4-TRE_L1) and pB254

(pENTR_L1-EYFP-4×MATP_L2) with pZDonor_3-GTW-4 in a Gateway LR reaction.

pB274 (pZD_Seq3-TRE-EYFP-4×PDCD4II-Seq4) was prepared by combining pZ251 (pENTR_L4-TRE_L1) and pB256 (pENTR_L1-EYFP-4×PDCD4II_L2) with pZDonor_3-GTW-4 in a Gateway LR reaction.

pB276 (pZD_Seq3-TRE-EYFP-4×PPARA-Seq4) was prepared by combining pZ251 (pENTR_L4-TRE_L1) and pB258 (pENTR_L1-EYFP-4×PPARA_L2) with pZDonor_3-GTW-4 in a Gateway LR reaction.

pB278 (pZD_Seq3-TRE-EYFP-4×RECKII-Seq4) was prepared by combining pZ251 (pENTR_L4-TRE_L1) and pB260 (pENTR_L1-EYFP-4×RECKII_L2) with pZDonor_3-GTW-4 in a Gateway LR reaction.

pB046 (pZD_Seq5-5×UAS-iRFP-miR-21-Seq6) was prepared by combining pZ296 (pENTR_L4-5×UAS_L1) and pB045 (pENTR_L1-iRFP-miR-21_L2) with pZDonor_5-GTW-6 in a Gateway LR reaction.

pZ316 (pZD_Seq2-hEF1α-RheoRec-2A-Rec-FF3-Seq3) was prepared by combining pZ529 (pENTR_L4-hEF1α_L1) (4) and pZ304 (pENTR_L1- RheoRec-2A-Rec-FF3_L2) with pZDonor_2-GTW-3 in a Gateway LR reaction.

All of the primers used in plasmid construction are listed in Table S1.

1. Xie Z, Wroblewska L, Prochazka L, Weiss R, Benenson Y (2011) Multi-input RNAi-based logic circuit for identification of specific cancer cells. *Science* 333(6047):1307–1311.
2. Bleris L, et al. (2011) Synthetic incoherent feedforward circuits show adaptation to the amount of their genetic template. *Mol Syst Biol* 7:519.
3. Hahne F, et al. (2009) flowCore: A Bioconductor package for high throughput flow cytometry. *BMC Bioinformatics* 10:106.
4. Guye P, Li Y, Wroblewska L, Duportet X, Weiss R (2013) Rapid, modular and reliable construction of complex mammalian gene circuits. *Nucleic Acids Res* 41(16):e156.
5. Leisner M, Bleris L, Lohmueller J, Xie Z, Benenson Y (2010) Rationally designed logic integration of regulatory signals in mammalian cells. *Nat Nanotechnol* 5(9):666–670.
6. Chen Y, et al. (2008) MicroRNA-21 down-regulates the expression of tumor suppressor PDCD4 in human glioblastoma cell T98G. *Cancer Lett* 272(2):197–205.

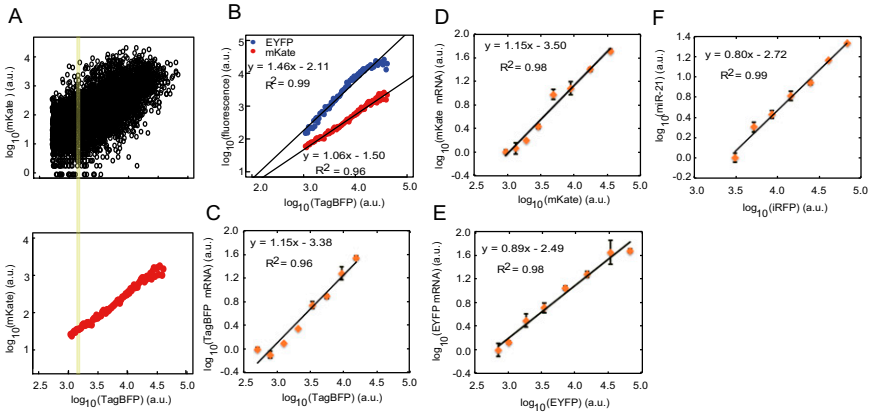

Fig. S1. Binning process of FACS data and the correlation between fluorescent intensities and miRNA/mRNA levels. (*A*) An example of the binning process of FACS data. *Top* plot represents an example of raw FACS data. The yellow bar represents an example of the binning process that is sorted by TagBFP. Red circles in *Bottom* plot represent mean values of the indicated fluorescence. (*B*) The linear relationship of different fluorescent intensities. Black lines represent the linear regression lines of TagBFP vs. EYFP (blue circles) and TagBFP vs. mKate (red circles). (*C–F*) The positive linear correlation between TagBFP (*C*), mKate (*D*), EYFP (*E*), and iRFP (*F*) fluorescent intensities and the corresponding miRNA or mRNA levels measured by qRT-PCR, respectively.

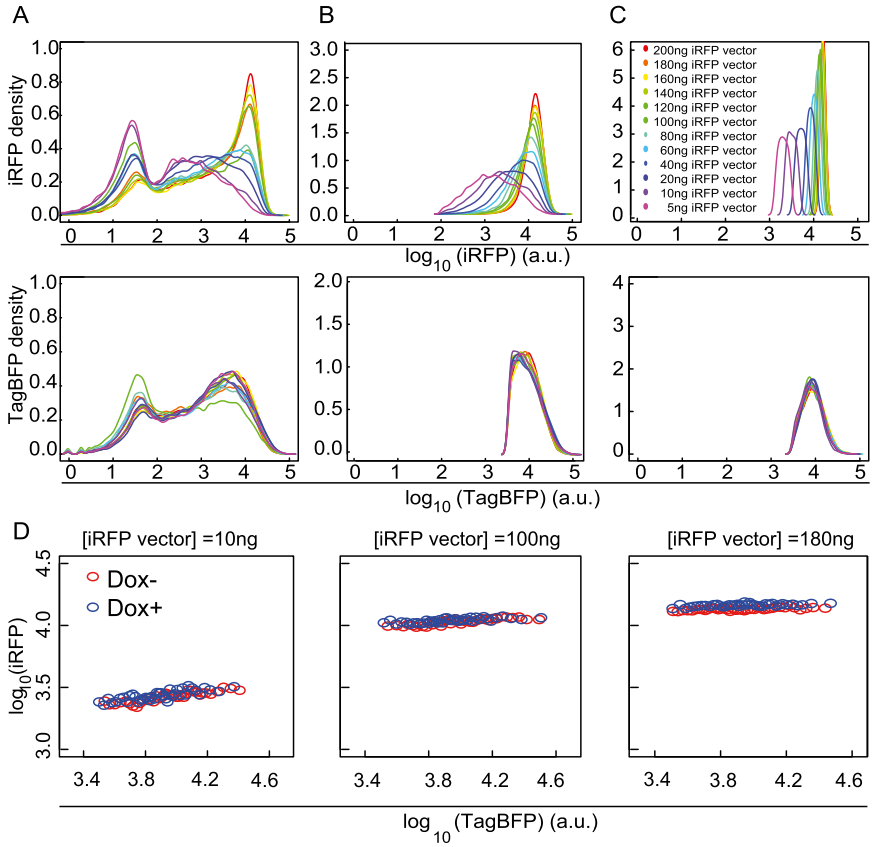

Fig. S2. The processing procedure for FACS data. Colored lines represent density distributions of cells transfected with various amounts of iRFP plasmid. (*A*) Histogram of the raw iRFP and TagBFP FACS data. (*B*) Histogram of the iRFP and TagBFP gated with iRFP > 0 and TagBFP > 3,000. (*C*) Cells whose iRFP value ranked from 45% to 70% of all data in *B* were selected for analysis. These gated cells had an approximately equal mean value of TagBFP normal distribution, but displayed a gradually increased mean value of iRFP normal distribution with increasing amount of the iRFP plasmid in the transfection experiment. (*D*) The correlation between TagBFP and iRFP of the processed FACS data. The three panels from *Left* to *Right* corresponded to the 2nd, 7th, and 11th panels in Fig. 2*C*.

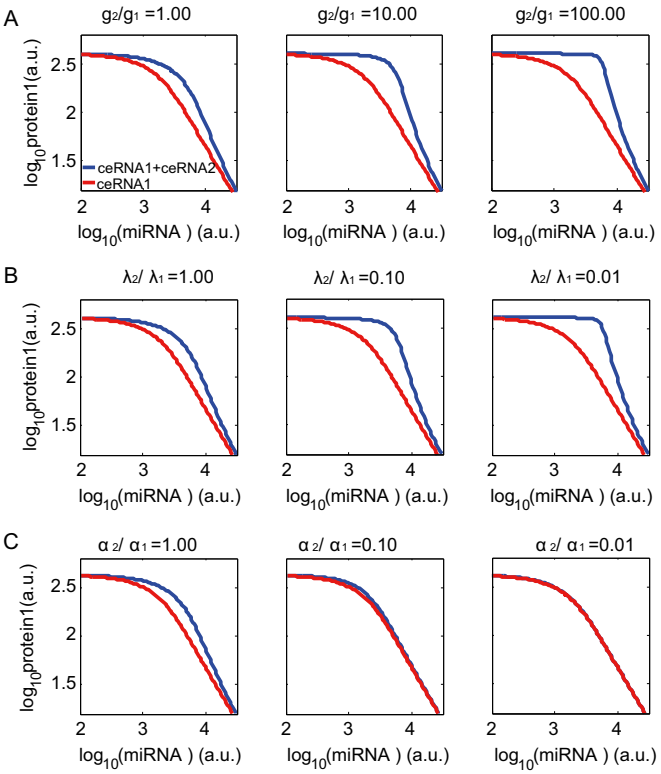

Fig. S3. Nonreciprocal competition between perfectly and partially paired targets. (*A*) Simulated protein1 level as a function of miRNA expression level. In each panel, we assumed that ceRNA1 and ceRNA2 had an identical transcription level, but different ratios of the complex degradation rate g_2/g_1. We assumed that perfectly paired targets had a larger complex degradation rate than partially paired targets (1). (*B*) Simulated protein1 level as a function of miRNA expression level. In each panel, we assumed that ceRNA1 and ceRNA2 had an identical transcription level, but different ratios of the miRNA binding ability λ_2/λ_1. Perfect pairing released the largest amount of free energy, resulting in the smallest λ (Fig. 3*F*). (*C*) Simulated protein1 level as a function of miRNA expression level. In each panel, we assumed that ceRNA1 and ceRNA2 had an identical transcription level, but different ratios of the miRNA loss rate α_2/α_1.

1. Haley B, Zamore PD (2004) Kinetic analysis of the RNAi enzyme complex. *Nat Struct Mol Biol* 11(7):599–606.

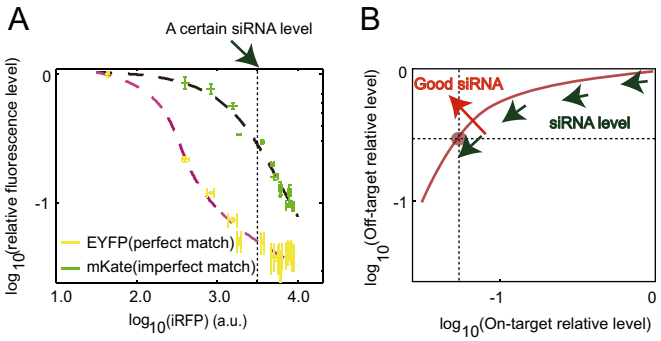

Fig. S4. miRNA repression efficiency on partially paired and perfectly paired targets. (*A*) Dose–response curve for miR-21 partially paired and perfectly paired targets. miR-21 simultaneously targeted mKate with partial complementary MREs and EYFP with perfect complementary MREs. (*B*) On-target–off-target relative repression curve. We named the mRNA with perfectly paired MRE as the on target and mRNA with partially paired MRE as the off target for the RNAi knockdown experiment. For a certain siRNA/miRNA level, we could get one EYFP (on-target) and one mKate (off-target) relative expression value as shown in *A*. The corresponding on-target relative level was set to be the abscissa value and the off-target relative level was treated as the ordinate value on the on-target–off-target relative repression plot, as shown by the pink circle in *B*. By varying the siRNA/miRNA level, we plotted the on-target–off-target relative repression curve as shown by the pink curve in *B*. The red arrow points to the "Good siRNA" region, where siRNA effectively represses on-target RNA but has little effect on off-target RNA.

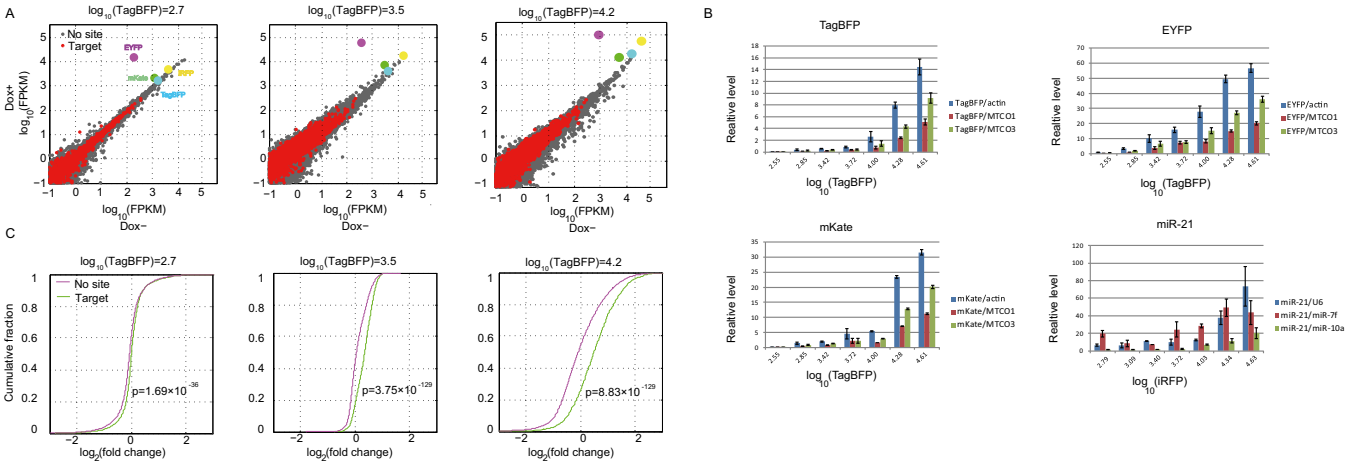

Fig. S5. The impact of exogenous ceRNA on natural miR-21 targets. (*A*) Scatter plot of FPKMs of transcripts from samples with or without Dox. We performed RNA-seq analysis on HEK293 cells transfected with the synthetic circuits. The cells were sorted into three groups according to the TagBFP fluorescent level with or without Dox, respectively. Red circles show the FPKMs of endogenous miR-21 targets predicted by TargetScan and gray circles show those of other genes. (*B*) qRT-PCR validation of synthetic gene expression. Cells were sorted according to TagBFP fluorescent value. The mRNA levels of TagBFP, EYFP, and mKate were compared with the mRNA of actin, MTCO1, and MTCO3 genes, respectively. The exogenous miR-21 level was compared with the endogenous miR-7f, miR-10a, and U6 snRNA, respectively. (*C*) Cumulative distributions of mRNA fold changes between samples with or without Dox for TargetScan predicted miR-21 targets (green line) and genes with no miR-21 target site (pink line). *P* value is calculated by a one-sided Kolmogorov–Smirnov (K-S) test.

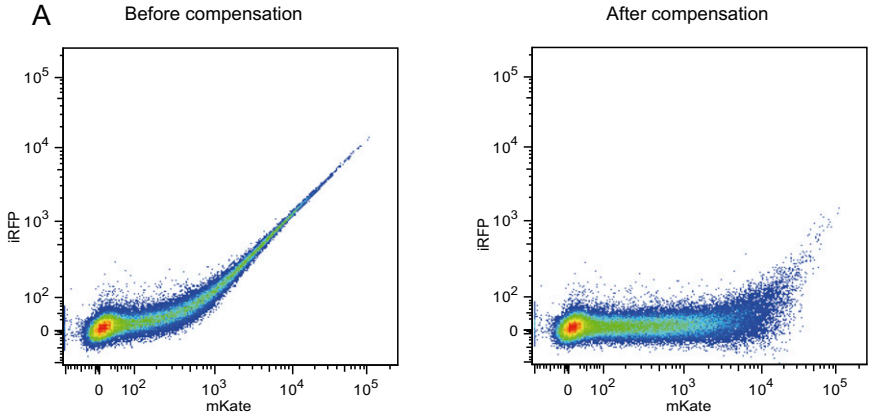

B

Channel / Fluorescence	iRFP	TagBFP	EYFP	mKate
iRFP		0.0	0.0	0.0
TagBFP	0.0		0.0	0.0
EYFP	0.0	0.0		0.0
mKate	11.8%	0.1%	0.0	

Fig. S6. Compensation on flow cytometry. (*A*) Compensation effect between mKate and iRFP. We measured the iRFP channel signal while we transfected only cells with mKate plasmid. The *y* axis represents the value from the iRFP channel and the *x* axis represents the value from the mKate channel. *Left* panel shows the raw data. *Right* panel shows the compensated data. (*B*) Compensation between different fluorescent proteins. Based on single-color positive control as shown in *A*, we estimated that 11.8% of mKate spilt into the iRFP channel and 0.1% of mKate spilt into the TagBFP channel. We calculated the compensated iRFP value as $(\text{iRFP} - 11.8\% \times \text{mKate})$ in each cell event and ignored the mKate spilt over into the TagBFP channel.

Table S1. Information of oligonucleotides used in this study

Name	Primer sequences
For vector construction	
p1	AATTTCTCGAGTTAATTAAACTAGTGGCGCGCCG
p2	AATTCGGCGCGCCACTAGTTTAATTAACTCGAGA
p3	GGCCGCCTCAGATCTCGAGCTCA
p4	AGCTTGAGCTCGAGATCTGAGGC
p5	GGGGACAAGTTTGTACAAAAAAGCAGGCTGATCGCCACCATGGTGTC
p6	GGGGACCACTTTGTACAAGAAAGCTGGGTACCCGGGTTGCGGCCGCATCAATTAAGTTTGTGCCCC
p7	GGGGACAAGTTTGTACAAAAAAGCAGGCTGATTACCGGTCGCCACCATG
p8	GGGGACCACTTTGTACAAGAAAGCTGGGTAGATCAGTTATCTAGATCCGGTGG
p9	TTTGCTAGCTTACCGGTCGCCACCATGGTGAGC
p10	TTTGCTAGCTGGGCCTGGGTTCTCCTCCACGTCGCCGGCCTGCTTCAGCAGAGAGAAGTTGGTGGCGCCAGATCCCTTGTACAGCTCG-TCCATGC
p11	TTTACTAGTATGACCGAGTACAAGCCCACG
p12	TTTGCGGCCGCTCAGGCACCGGGCTTGCGG
p13	TTTACCGGTACCATGTCTAGACTGGACAAG
p14	TTGCTAGCACTAGTTGGGCCTGGGTTCTCCTCCACGTCGCCGGCCTGCTTCAGCAGAGAGAAGTTGGTGGCGCCAGATCCCCCGGGG-AGCATGTCAAGG
p15	TTTACCGGTCGCCACCATGAGCG
p16	TTTGCGGCCGCTTAGTGCCCCAGTTTGCTAGG
p17	TTTGCGGCCGCCAGGTGAGTCCAGTTTTCTTGCCGTTCTGTAAG
p18	TTAAGCTTCCTGAAGGTCAAGTAACAGTCATACAGCTAGAAAAGTCCCTGAAAAAAAGAATTAGTTAAGAAG
p19	GGCCGCAAACGATATGGGCTGAATACAATACCAAACGATATGGGCTGAATACAATACCAAACGATATGGGCTGAATACAATACCA-AACGATATGGGCTGAATACAATACA
p20	AGCTTGTATTGTATTCAGCCCATATCGTTTGGTATTGTATTCAGCCCATATCGTTTGGTATTGTATTCAGCCCATATCGTTTGGTATTGT-ATTCAGCCCATATCGTTTGC
p21	GGGGACAAGTTTGTACAAAAAAGCAGGCTGAACCATGTCTAGACTGGACAAGAGC
p22	GGGGACCACTTTGTACAAGAAAGCTGGGTAGATCAGTTATCTAGATCCGGTGG
b13009	GGCCAGTGGAATATTCTAATAAGCTACCTTTTGTAAGTGCCATGTTTAAGTGGAATATTCTAATAAGCTACCTTTTGTAAG
b13010	GGCACTTACAAAAGGTAGCTTATTAGAATATTCCACTTAAACATGGCACTTACAAAAGGTAGCTTATTAGAATATTCCACT
b13011	TGCCATGTTTAAGTGGAATATTCTAATAAGCTACCTTTTGTAAGTGCCATGTTTAAGTGGAATATTCTAATAAGCTA
b13012	TCGATAGCTTATTAGAATATTCCACTTAAACATGGCACTTACAAAAGGTAGCTTATTAGAATATTCCACTTAAACAT
b13021	CTGCCATGTTTAAGTGGAATATTCTAATAAGCTACCTTTTGTAAGTGCCATGTTTAAGTGGAATATTCTAATAAGCTA
b13022	TTATTAGAATATTCCACTTAAACATGGCACTTACAAAAGGTAGCTTATTAGAATATTCCACTTAAACATGGCAGGTAC
b13023	CCTTTTGTAAGTGCCATGTTTAAGTGGAATATTCTAATAAGCTACCTTTTGTAAGTGCCATGTTTA
b13024	CATGGCACTTACAAAAGGTAGCTTATTAGAATATTCCACTTAAACATGGCACTTACAAAAGGTAGC
b13025	AGTGGAATATTCTAATAAGCTATCGATTGTAAGTGCCAGCGGCCGCGTCGAC
b13026	CCGGGTCGACGCGGCCGCTGGCACTTACAATCGATAGCTTATTAGAATATTCCACTTAAA
b13070	GGCCGCTTATTTTGCTTTTGTATAAGCTGCCTTTTGTAAGTGCCATGTTTATTATTTTGCTTTTGTATAAGCTGCCTTTTGTA
b13071	CACTTACAAAAGGCAGCTTATACAAAAGCAAAATAATAAACATGGCACTTACAAAAGGCAGCTTATACAAAAGCAAAATAAGC
b13072	AGTGCCATGTTTATTATTTTGCTTTTGTATAAGCTGCCTTTTGTAAGTGCCATGTTTATTATTTTGCTTTTGTATAAGCTGC
b13073	CCGGGCAGCTTATACAAAAGCAAAATAATAAACATGGCACTTACAAAAGGCAGCTTATACAAAAGCAAAATAATAAACATGG
b13086	GGCCGCGGAATATTCTAATAAGCTACCTTCCTTTTGTAAGTGCCATGTTTAGGAATATTCTAATAAGCTACCTTCCTTTTGTA
b13087	CACTTACAAAAGGAAGGTAGCTTATTAGAATATTCCTAAACATGGCACTTACAAAAGGAAGGTAGCTTATTAGAATATTCCGC
b13088	AGTGCCATGTTTAGGAATATTCTAATAAGCTACCTTCCTTTTGTAAGTGCCATGTTTAGGAATATTCTAATAAGCTACCTTC
b13089	CCGGGAAGGTAGCTTATTAGAATATTCCTAAACATGGCACTTACAAAAGGAAGGTAGCTTATTAGAATATTCCTAAACATGG
b13102	GGCCGCGTCTCACAGTTTGAAATAAGCTACCTTTTGTAAGTGCCATGTTTAGTCTCACAGTTTGAAATAAGCTACCTTTTGTA
b13103	CACTTACAAAAGGTAGCTTATTTCAAACTGTGAGACTAAACATGGCACTTACAAAAGGTAGCTTATTTCAAACTGTGAGACGC
b13104	AGTGCCATGTTTAGTCTCACAGTTTGAAATAAGCTACCTTTTGTAAGTGCCATGTTTAGTCTCACAGTTTGAAATAAGCTAC
b13105	CCGGGTAGCTTATTTCAAACTGTGAGACTAAACATGGCACTTACAAAAGGTAGCTTATTTCAAACTGTGAGACTAAACATGG
b13035	CGCGGGCCCGGGATCCACCGGAGTAC
b13036	TCCGGTGGATCCCGGGCCCGCGGTAC
ch-5	TTAACCGGTATGGCTGAAGGATCCGTCGC
b12009	TTTGCGGCCGCTCACTCTTCCATCACGCCGATC
b13078	GGCCGCATTGACTTCAAGATAATAAGCTGCTCCTTTTGTAAGTGCCATGTTTAATTGACTTCAAGATAATAAGCTGCTCCTTTTGTA
b13079	CACTTACAAAAGGAGCAGCTTATTATCTTGAAGTCAATTAAACATGGCACTTACAAAAGGAGCAGCTTATTATCTTGAAGTCAATGC
b13080	AGTGCCATGTTTAATTGACTTCAAGATAATAAGCTGCTCCTTTTGTAAGTGCCATGTTTAATTGACTTCAAGATAATAAGCTGCTC
b13081	CCGGGAGCAGCTTATTATCTTGAAGTCAATTAAACATGGCACTTACAAAAGGAGCAGCTTATTATCTTGAAGTCAATTAAACATGG
b13094	GGCCGCAAAAAATCTGTTAGATAAGCTACCTTTTGTAAGTGCCATGTTTAAAAAAATCTGTTAGATAAGCTACCTTTTGTA
b13095	CACTTACAAAAGGTAGCTTATCTAACAGATTTTTTTAAACATGGCACTTACAAAAGGTAGCTTATCTAACAGATTTTTTGC
b13096	AGTGCCATGTTTAAAAAAATCTGTTAGATAAGCTACCTTTTGTAAGTGCCATGTTTAAAAAAATCTGTTAGATAAGCTAC
b13097	CCGGGTAGCTTATCTAACAGATTTTTTTAAACATGGCACTTACAAAAGGTAGCTTATCTAACAGATTTTTTTAAACATGG

Table S1. Cont.

Name	Primer sequences
For RT-PCR	
b13032-EYFP-F	TGAAGCAGCACGACTTCTTCAAGTC
b13033-EYFP-R	TGTTGTGGCGGATCTTGAAGTTC
b13039-mKate-F	TGGAGGGCACCGTGAACAACCAC
b13040-TagBFP-F	TGGAGGGCACCGTGGACAACCAT
b13041-mKate-R	GGTTTTGCTGCCGTACATGAAGCTG
b13042-TagBFP-R	GGTCTTGCTGCCGTAGAGGAAGCTA
ch66-miR21-F	CCTAGCTTATCAGACTGATGTTGAAAA
ch77-R	ATCGAGCACCAGTTACGCATGCCG
ch78-U6-F	CCTCGTGAAGCGTTCCATATTCTAAA
Actin-F	GCTCGTCGTCGACAACGGCTC
Actin-R	CAAACATGATCTGGGTCATCT
b14001-miR18a-F	CCTAAGGTGCATCTAGTGCAGATAGAAA

Table S2. Transfection configuration

Plasmid DNA	Amount					
Used in Fig. 2 and Fig. S2						
pCAG-rtTA-2A-Puro-FF5, ng	100					
pCAG-TagBFP-FF5, ng	100					
phEF1α-mKate-4×PDCD4, ng	50					
pTRE-EYFP-4×PDCD4, ng	50					
phEF1α-iRFP-miR-21, ng	*x*					
pDT7004, ng	200 − *x*					
x = 5, 10, 20, 40, 60, 80, 100, 120, 140, 160, 180, 200						
Final concentration of Dox, ng/mL	*y*					
y = 0, 200						
Used in Fig. 3*B*						
pDT7004, ng	60	60	60	60	60	
pCAG-rtTA-2A-Puro-FF5, ng	100	100	100	100	100	
pCAG-TagBFP-FF5, ng	100	100	100	100	100	
phEF1α-mKate-4×PDCD4, ng	100	100	100	100	100	
pTRE-EYFP-MCS, ng	100					
pTRE-EYFP-1×PDCD4, ng		100				
pTRE-EYFP-4×PDCD4, ng			100			
pTRE-EYFP-8×PDCD4, ng				100		
pTRE-EYFP-12×PDCD4, ng					100	
phEF1α-iRFP-miR-21, ng	40	40	40	40	40	
Final concentration of Dox, ng/mL	*y*	*y*	*y*	*y*	*y*	
y = 0, 200						
Used in Fig. 3*E*						
pDT7004, ng	60	60	60	60	60	60
pCAG-rtTA-2A-Puro-FF5, ng	100	100	100	100	100	100
pCAG-TagBFP-FF5, ng	100	100	100	100	100	100
phEF1α-mKate-4×PDCD4, ng	100	100	100	100	100	100
pTRE-EYFP-4×BMPR, ng	100					
pTRE-EYFP-4×MTAP, ng		100				
pTRE-EYFP-4×PDCD4, ng			100			
pTRE-EYFP-4×PDCD4II, ng				100		
pTRE-EYFP-4×PPARA, ng					100	
pTRE-EYFP-4×RECK, ng						100
phEF1α-iRFP-miR-21, ng	40	40	40	40	40	40
Final concentration of Dox, ng/mL	*y*	*y*	*y*	*y*	*y*	*y*
y = 0, 200						
Used in Fig. 4						
pCAG-rtTA-2A-Puro-FF5, ng	100	100	100			
pCAG-TagBFP-FF5, ng	100	100	100			
phEF1α-mKate-4×PDCD4, ng	50	50	50			
pTRE-EYFP-4×PDCD4, ng	0	50	80			
phEF1α-iRFP-miR-21, ng	*x*	*x*	*x*			
pDT7004, ng	250 − *x*	200 − *x*	170 − *x*			
x = 2.5, 5, 7.5, 10, 20, 40, 60, 80, 100, 120						
Final concentration of Dox, ng/mL	*y*	*y*	*y*			
y = 0, 200						
Used in Fig. 5*B* and Fig. S4						
pCAG-rtTA-2A-Puro-FF5, ng	100					
pCAG-TagBFP-FF5, ng	100					
phEF1α-mKate-4×PDCD4, ng	50					
pTRE-EYFP-4×T21, ng	50					
phEF1α-iRFP-miR-21, ng	*x*					
pDT7004, ng	200 − *x*					
x = 0, 5, 10, 20, 40, 60, 80, 100, 120, 140, 160, 180, 200						
Final concentration of Dox, ng/mL	*y*					
y = 0, 200						
Used in Fig. 5*C*						
pCAG-rtTA-2A-Puro-FF5, ng	100	100	100	100		
pCAG-TagBFP-FF5, ng	100	100	100	100		
phEF1α-mKate-4×PDCD4, ng	50	80	110			
phEF1α-mKate-MCS, ng				110		

Table S2. Cont.

Plasmid DNA	Amount			
pTRE-EYFP-4×T21, ng	50	50	50	50
phEF1α-iRFP-miR-21, ng	*x*	*x*	*x*	*x*
pDT7004, ng	200 − *x*	170 − *x*	140 − *x*	140 − *x*
x = 0, 1.25, 2.5, 5, 10, 20, 40, 60, 80, 100, 120, 140				
Final concentration of Dox, ng/mL	*y*	*y*	*y*	*y*
y = 0, 200				
Used in Fig. 5*D*				
pCAG-rtTA-2A-Puro-FF5, ng	100	100	100	100
pCAG-TagBFP-FF5, ng	100	100	100	100
phEF1α-mKate-4×BMPR, ng	110			
phEF1α-mKate-4×PDCD4, ng		110		
phEF1α-mKate-4×RECK, ng			110	
phEF1α-mKate-MCS, ng				110
pTRE-EYFP-4×T21, ng	50	50	50	50
phEF1α-iRFP-miR-21, ng	*x*	*x*	*x*	*x*
pDT7004, ng	140 − *x*	140 − *x*	140 − *x*	140 − *x*
x = 0, 1.25, 2.5, 5, 10, 20, 40, 60, 80, 100, 120, 140				
Final concentration of Dox, ng/mL	*y*	*y*	*y*	*y*
y = 0, 200				
Used in Fig. S1 *A* and *B*				
pCAG-rtTA-2A-Puro-FF5, ng	100			
pCAG-TagBFP-FF5, ng	100			
phEF1α-mKate-4×PDCD4, ng	50			
pTRE-EYFP-4×PDCD4, ng	50			
phEF1α-iRFP-miR-21, ng				
pDT7004, ng	200			
Final concentration of Dox, ng/mL	200			
Used in Figs. S1 *C*–*F* and S5*B*				
pDT7004, ng	100	300		
pCAG-rtTA-2A-Puro-FF5, ng	100			
pCAG-TagBFP-FF5, ng	100			
phEF1α-mKate-4×PDCD4, ng	100			
TRE-EYFP-4×PDCD4, ng	100			
phEF1α-iRFP-miR-21, ng		200		
Final concentration of Dox, ng/mL	200			
Used in Fig. S5 *A* and *C*				
pCAG-rtTA-2A-Puro-FF5, ng	100			
pCAG-TagBFP-FF5, ng	100			
phEF1α-mKate-4×PDCD4, ng	100			
pTRE-EYFP-4×PDCD4, ng	100			
phEF1α-iRFP-miR-21, ng	100			
Final concentration of Dox, ng/mL	*y*			
y = 0, 200				
Used in Fig. S6				
pDT7004, ng	450			
phEF1α-mKate-4×PDCD4	50			

Table S3. Fit parameters

Parameter	Value, Fig. 2*C*	Value, Fig. 3*B*	Value, Fig. 3*E*
K_m	0.65	0.36	0.35
B_m	1.66	2.50	2.61
K_e	1.09	0.99	0.74
B_e	2.05	1.70	2.28
K_t	2.05	2.20	2.20
B_t	1.60	0.35	0.49
K_1	2.27	1.50	1.50
K_2	3.20	5.00	4.50
λ_1	5.68	4.01	4.00
λ_2	6.00	Shown in Fig. 3*C*	Shown in Fig. 3*F*
σ	1.25	1.00	1.00
θ_1	Shown in Fig. 2*C*	103.98	137.00